Theory of Rayleigh scattering from metallic carbon nanotubes

Ermin Malić,[1,][*] Matthias Hirtschulz,[1] Frank Milde,[1] Yang Wu,[2] Janina Maultzsch,[2] Tony F. Heinz,[2]
Andreas Knorr,[1] and Stephanie Reich[3]

[1]*Institut für Theoretische Physik, Nichtlineare Optik und Quantenelektronik, Technische Universität Berlin, 10623 Berlin, Germany*
[2]*Department of Physics and Department of Electrical Engineering, Columbia University, New York, New York 10027, USA*
[3]*Fachbereich Physik, Freie Universität Berlin, 14195 Berlin, Germany*

We present a microscopic calculation of the Rayleigh (elastic light) scattering spectra for single-walled carbon nanotubes. Combining density-matrix formalism and the tight-binding model, we obtain results for nanotubes of arbitrary chiral index. In agreement with experiment, the calculated Rayleigh spectra of metallic nanotubes show a double-peaked structure resulting from the trigonal warping effect, with the low-energy feature exhibiting greater intensity. We explain the intensity ratios by the wave-vector dependence of the optical matrix elements. Also in accord with experiment, the Rayleigh line shape of each peak is asymmetric, with an enhanced cross section for lower photon energies. This behavior arises from contributions of the nonresonant optical susceptibility to the Rayleigh scattering process.

The characterization of specific single-walled carbon nanotubes is a substantial challenge for current research. Nanotubes, as prototypical one-dimensional systems, show well-defined optical transitions that can be exploited for structural assignment. In addition to the established methods of optical spectroscopy, such as absorption, photoluminescence, and Raman spectroscopy,[1–4] Rayleigh scattering has recently emerged as a characterization technique for individual single-walled carbon nanotubes (SWCNTs).[5–7] Similarly to other optical methods Rayleigh scattering spectroscopy provides information about the nanotube structure through resonant enhancement of the elastically scattered light when the photon energy matches that of an electronic transition. An advantage of Rayleigh scattering lies in its ability to uncover the optical properties of *individual* nanotubes.[5] Optical absorption, in contrast, is challenging for individual nanosystems, because the sample (e.g., single tubes and nanoparticles) changes the intensity of the incoming light by $\sim 10^{-5}$–10^{-4}. Scattering techniques measure an absolute signal instead of a fractional change. In this respect Rayleigh scattering (elastic light scattering) is similar to Raman scattering (inelastic scattering). However, to obtain the optical properties from a Raman experiment we need to record many spectra with varying laser energy.[3,4] The most widely used optical technique for studying single-walled carbon nanotubes is photoluminescence.[1,2] However, it is limited to semiconducting tubes with smaller diameters. Rayleigh scattering offers rapid data collection, an assignment of (n_1, n_2) chirality, and it is applicable to both semiconducting and metallic tubes. It has been used to confirm the electronic structure of nanotubes (trigonal warping effect in metallic tubes), to study tube-tube interaction, and characterize individual tubes in combination with transport and electron-diffraction experiments.[5–7] This wealth of experimental studies has not yet been complemented by theoretical work.

In this paper, we study the Rayleigh scattering spectra of SWCNTs. We derive an expression for the Rayleigh scattering cross section per unit length using analytical results for the optical matrix elements of arbitrary (n_1, n_2) nanotubes

and transition energies within the tight-binding approximation. The theory is applied to the features of the Rayleigh scattering spectra for metallic nanotubes with diameters of approximately 2 nm, since these nanotubes have been investigated experimentally.[6] The comparison of tight-binding and density functional theory calculations has shown that the tight-binding method is suitable for the description of such large nanotubes.[8] Working within the free-particle model, we can understand the intensity ratio of the double-peaked structure as a consequence of the trigonal warping effect. This effect describes the deviation of the equienergy contours from circles in the Brillouin zone of graphene around the *K* point.[9,10] As discussed below Eq. (5), the inclusion of excitonic effects will somewhat modify the Rayleigh line shape, but is not expected to change the characteristic features, such as the enhanced strength of the lower-energy component of the split metallic peaks.

We first outline the calculation of the Rayleigh scattering cross section $\sigma(\omega)$ for carbon nanotubes. Treating Rayleigh scattering from SWCNTs as electromagnetic scattering from a long cylinder with a diameter small compared to the wavelength of light, we can write the scattering cross section per unit length as[5,11]

$$\sigma(\omega) \propto r^4 \omega^3 |\chi(\omega)|^2, \tag{1}$$

where ω is the angular frequency of the light and r the radius of the cylinder. The cross section $\sigma(\omega)$ is given by the ratio of the rate $W_s = \int_A \mathbf{S}_s \cdot \mathbf{e}_r dA$ at which energy passes through the scattering surface A and the incident irradiance I_i.[11] The scattering direction is denoted by $\mathbf{e}_r$, and $\mathbf{S}_s = \frac{1}{2}\mathrm{Re}[\mathbf{E}_s \times \mathbf{H}_s^*]$ is the Poynting vector of the scattered field. From the Maxwell equations, one derives expression for $\sigma(\omega)$ in Eq. (1) by solving the wave equation in cylindrical coordinates, taking the appropriate limit of the diameter of the nanotube being much smaller than the wavelength of light. Here we consider the Rayleigh scattering cross section for incident light polarized along the nanotube axis, since this gives the dominant scattering response.[5]

Information about electronic properties of the nanotube enters into the Rayleigh scattering cross section through the frequency-dependent optical susceptibility[12] $\chi(\omega) = \varepsilon(\omega) - 1$, where $\varepsilon(\omega)$ denotes the effective dielectric function of the nanotube. The susceptibility $\chi(\omega)$ can be defined as the response function [current density $j(\omega)$ versus the external vector potential $A(\omega)$] of the perturbed system as follows:[13]

$$\chi(\omega) = \frac{j(\omega)}{\varepsilon_0 \omega^2 A(\omega)}. \tag{2}$$

To obtain $\chi(\omega)$, we calculate the current density $j(\omega)$, which depends on the Fourier transform of the microscopic polarization $\rho_{\boldsymbol{k}}(t)$ (probability amplitude for an optical transition at wave vector $\boldsymbol{k}$) and the optical matrix element $M_z(\boldsymbol{k})$ along the nanotube axis (z axis) as follows:[13,14]

$$j(t) \propto \frac{e_0}{2m_0} \sum_{ij} [\langle i|\boldsymbol{p} + e\boldsymbol{A}|j\rangle\langle a_i^+ a_j\rangle + c.c.]$$

$$= -i\frac{2e_0\hbar}{m_0} \sum_{\boldsymbol{k}} \mathrm{Re}[M_z(\boldsymbol{k})\rho_{\boldsymbol{k}}(t)]. \tag{3}$$

Here $|i\rangle$ is the electronic state described by the compound index $i = (\boldsymbol{k}, x)$, where $x = c, v$ stands for the conduction (c) or the valence band (v), and $\boldsymbol{k}$ denotes the two-dimensional graphene wave vector. The annihilation a_i and creation operators a_j^+ act on an electron in the state $|i\rangle$. In Eq. (3), m_0 is the bare electron mass, e_0 is the elementary charge, and $\boldsymbol{p} = \frac{\hbar}{i}\nabla_{\boldsymbol{k}}$ is the linear momentum operator. Within the tight-binding model and the orthogonal first-neighbor approximation,[9,15–17] we obtain a fully analytical expression for the optical matrix element $M_z(\boldsymbol{k})$ for light polarized along the nanotube axis as a function of the chiral index (n_1, n_2) as follows:[13]

$$M_z(m, k_z) = \frac{M_c}{2\sqrt{N}|e(\boldsymbol{k})|}[(n_1 - n_2)\cos\Psi_3 - (2n_1 + n_2)\cos\Psi_1$$

$$+ (n_1 + 2n_2)\cos\Psi_2]. \tag{4}$$

Here $\boldsymbol{k}$ is defined by the band index m and the wave vector k_z along the nanotube axis; M_c denotes the optical matrix element for the two nearest-neighbor atoms which can be approximated to the constant value 0.7 within the tight-binding approximation.[13,18] Furthermore, it is $N = n_1^2 + n_2^2 + n_1 n_2$, and $\Psi_1 = \pi m\frac{2n_1 + n_2}{N} - 2\pi\frac{n_2}{q}k_z$, $\Psi_2 = \pi m\frac{n_1 + 2n_2}{N} + 2\pi\frac{n_1}{q}k_z$, with $\Psi_3 = \Psi_1 - \Psi_2$, and $|e(\boldsymbol{k})| = \sqrt{\sum_{i=1}^{3}[1 + 2\cos(\Psi_i)]}$. The number of graphene hexagons in the nanotube unit cell is denoted by q.[15]

Figure 1(a) shows the dependence of the optical matrix element $M_z(\boldsymbol{k})$ [Eq. (4)] on the band index m at the Γ point of zigzag nanotubes ($k_z = 0$), at which the subband transitions take place. This plot corresponds to the ΓKM high-symmetry line of graphene [Fig. 1(b)]. Note that the matrix element $M_z(m, 0)$ has a smaller absolute value on the ΓK than on the KM side. This will influence the oscillator strength of transitions. Depending on the side on which the corresponding
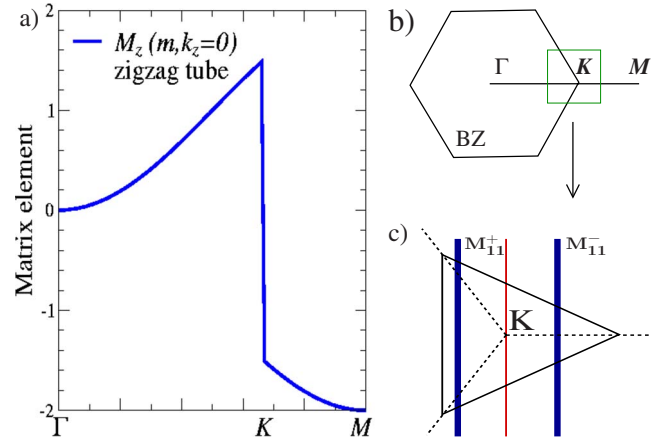

FIG. 1. (Color online) (a) Optical matrix element $M_z(\boldsymbol{k})$ along the high-symmetry line ΓKM of graphene corresponding to confined states of zigzag nanotubes. (b) Brillouin zone of graphene with the high-symmetry line ΓKM. (c) Simplified triangular energy contour of graphene around the K point of the Brillouin zone. The deviation from the circle is exaggerated to illustrate the trigonal warping. The vertical lines are the allowed wave vector lines corresponding to the lowest van Hove singularities of a metallic zigzag nanotube. The dashed lines indicate the three KM directions.

van Hove singularity is located with respect to the K point [Fig. 1(c)], the transition is expected to be stronger or weaker in intensity, as discussed below.

The calculation of the cross section $\sigma(\omega)$ requires, further, the determination of the microscopic polarization $\rho_{\boldsymbol{k}}$ [in Eq. (3)] as a function of the vector potential $A(\omega)$. Within the density matrix theory formalism, we obtain the following free-particle Bloch equation for $\rho_{\boldsymbol{k}}(t)$ (Ref. 12):

$$\dot{\rho}_{\boldsymbol{k}}(t) = -i\Delta\omega_{\boldsymbol{k}}\rho_{\boldsymbol{k}}(t) + g_{\boldsymbol{k}}(t) - \gamma\rho_{\boldsymbol{k}}(t). \tag{5}$$

The polarization is determined by three contributions: (1) the subband transition frequency $\Delta\omega_{\boldsymbol{k}} = [\omega_c(\boldsymbol{k}) - \omega_v(\boldsymbol{k})]$, (b) the quantity $g_{\boldsymbol{k}}(t) = \frac{e_0}{m_0}M_z(\boldsymbol{k})A(t)$ related to the Rabi frequency, and (3) the phenomenological parameter γ introduced to describe dephasing, resulting from electron-phonon or other interactions. It is important for computational convergence. Its value (Ref. 13) determines the linewidth in the calculated spectra and is taken in this work to be $\gamma = (0.0125/\hbar)$ eV. As a first approximation, we focus on the free-particle Bloch equations. In other theoretical studies, excitons have been described by solving the Bethe-Salpeter equation and applying the GW method.[19–23] For semiconducting nanotubes, excitonic transitions have been shown to dominate observed spectra[25,26] and even for metallic nanotubes bound excitons have been predicted.[21] Preliminary calculations including excitonic effects within the density matrix formalism show that both the subband transition energy and the Rabi frequency are renormalized, leading to a net blueshift of the free spectra.[24] However, the asymmetry of the double-peaked structure in the Rayleigh spectra of metallic nanotubes with its characteristic behavior in the intensity ratio remains unchanged. Excitonic interactions merely enhance these features. Therefore, analysis of free-particle transitions provides
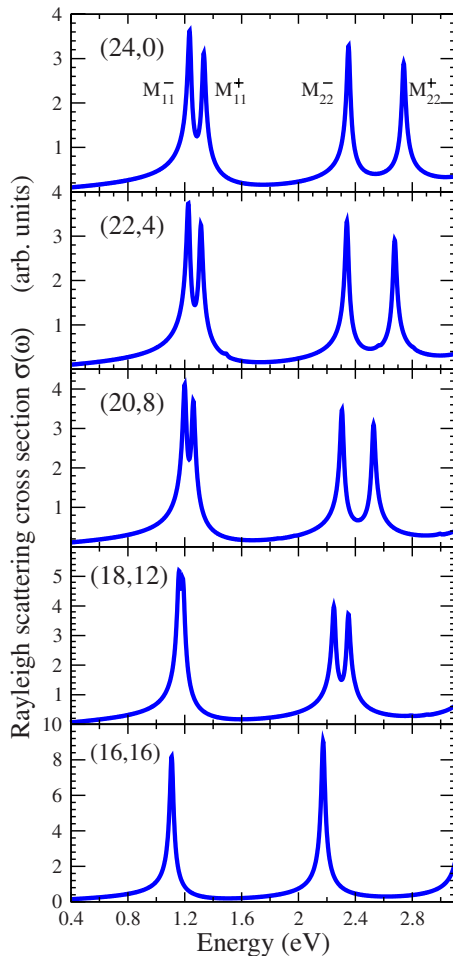
FIG. 2. (Color online) Rayleigh spectra of metallic nanotubes with a diameter of ~2 nm corresponding to the Kataura branch (Ref. 28) with $2n_1 + n_2 = 48$. The chiral angle increases from top to bottom. The figure illustrates the peak splitting caused by the trigonal warping effect that diminishes with increasing chiral angle (toward the armchair configuration) and increasing transition energy (Refs. 9 and 10).

FIG. 3. (Color online) Intensity ratios of transitions M_{11}^- and M_{11}^+, and of M_{22}^- and M_{22}^+ as a function of the chiral angle.

an important step in understanding the optical properties of carbon nanotubes, especially their chirality and family behavior.[13,18,27]

The Rayleigh scattering cross section $\sigma(\omega)$ in Eq. (1) is determined by the linear optical susceptibility $\chi(\omega)$. In this sense, it is similar to the optical absorption, which is also determined by this quantity. Unlike absorption, however, Rayleigh scattering has a contribution from the real part of $\chi(\omega)$ and, hence, includes effects from off-resonant optical transitions. This leads to important differences in the characteristics of Rayleigh and absorption spectra. Figure 2 shows the four lowest-lying transitions M_{11}^-, M_{11}^+, M_{22}^-, and M_{22}^+ in metallic carbon nanotubes with a diameter of approximately 2 nm. We focus on these nanotubes, since experimental Rayleigh spectra of SWCNTs with a similar diameter have already been measured.[5–7] Figure 2 illustrates three important features:

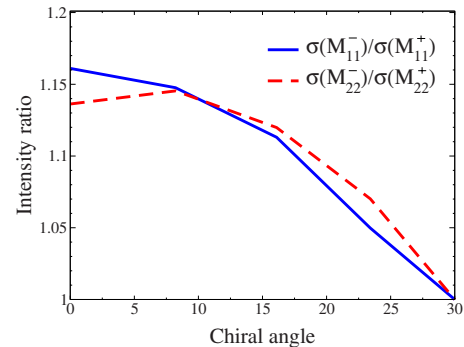(i) The Rayleigh scattering spectra of metallic nanotubes show a double-peaked structure that arises from trigonal warping. This effect describes the deviation of the equienergy contours from circles in the Brillouin zone of graphene around the K point [Fig. 1(c)]. The triangular shape of these equienergy contours makes it important on which side of the K point the van Hove singularities are located. As a result, there is peak splitting in the spectra of metallic nanotubes, as already known from absorption measurements.[15] The width of the splitting depends strongly on the chiral angle: It is maximal for zigzag tubes and decreases with increasing chiral angle, with no splitting present for the armchair configuration.[9,10] Figure 2 also confirms that the trigonal warping effect is larger at higher transition energies, as can be seen in the wider separation of the third and fourth peaks.

(ii) The relative intensities of the Rayleigh peaks have a distinctive behavior. For all nanotubes within a given Kataura branch, the lower-lying transition in the double-peaked structure is stronger in intensity, i.e., M_{11}^- is stronger than M_{11}^+, and M_{22}^- is stronger than M_{22}^+.

(iii) The Rayleigh spectra exhibit a slight enhancement of the scattering cross section at lower photon energies (see also Fig. 4).

The characteristic behavior of relative intensities in the double-peaked structure of metallic tubes in Fig. 2 has also been observed experimentally: the lower-energy peak of the split transition is always higher in intensity than the upper one.[7] Figure 3 demonstrates that this intensity difference decreases with the increasing chiral angle, connected to the decrease of the trigonal warping effect. At first sight, this seems to contradict the dependence of the density of states on chiral angle that has been shown to be enhanced for higher-lying transitions.[9] However, an explanation for the peak ratio is found in the interplay of the density of states with the optical matrix element $M_z(\mathbf{k})$. The oscillator strength of optical transitions is determined by both the density of states and the optical matrix element.[13] Especially for studies of the chirality dependence, it is important to consider the influence of the matrix element $M_z(\mathbf{k})$. As seen in Fig. 1, its absolute value is higher on the KM than on the ΓK side. The van Hove singularities located at the ΓK side lead to transitions at a higher energy[9] [Fig. 1(c)]. Since the absolute value of the matrix element is smaller on the ΓK branch, and since the cross section depends on the square of the matrix element [Eqs. (1)–(3)] the corresponding transition intensities are weaker, despite the enhanced density of the states.
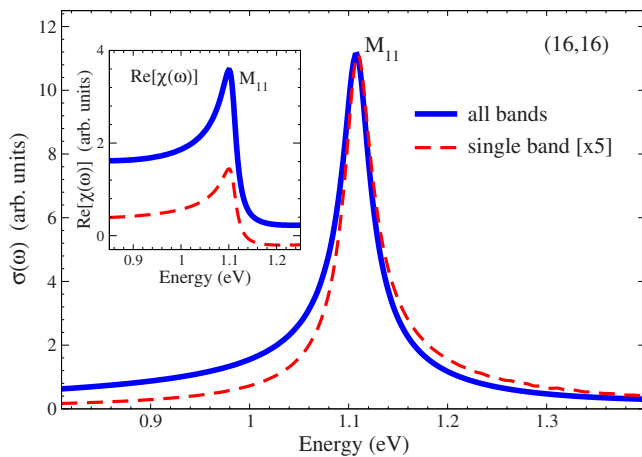
FIG. 4. (Color online) Asymmetry toward lower energies in the Rayleigh spectra. The cross section is plotted for the M_{11} transition of the (16,16) armchair nanotube. Single-band and all-band results are compared (the maxima are normalized to the value of the M_{11} peak in the all-band calculation) to illustrate that the enhancement of the Rayleigh scattering cross section at lower energies occurs only when the nonresonant response is included. The inset shows the corresponding real part of the susceptibility $\chi(\omega)$. Constructive interference of the nonresonant contribution in the low-energy wing of the resonant response accounts for the observed asymmetry.

In agreement with experimental results,[5–7] the Rayleigh peaks in Fig. 2 have an asymmetry toward lower energies, i.e., the scattering cross section is enhanced at lower energies. To see this more clearly we plot in Fig. 4 the cross section $\sigma(\omega)$ for the first (M_{11}) transition of the (16,16) armchair nanotube on an expanded energy scale. The dotted-dashed line shows results from a single-band calculation. We see that the characteristic asymmetry is observed only when all subband transitions are taken into consideration (solid line). An explanation for the enhanced Rayleigh scattering cross section at lower energies lies in the influence of the real part of the optical susceptibility $\chi(\omega)$. It has a long tail on the low-energy side of each transition, since the wing of the resonant response adds in phase with the nonresonant back-ground below the resonance, but interferes destructively above the resonance. The inset in Fig. 4 illustrates the behavior around the M_{11} transition of the (16,16) nanotube. The off-resonant contributions of higher subband transitions yield a background (solid line in the inset) that produces the observed asymmetry of Rayleigh peaks (Fig. 4). This interference effect from the nonresonant background also leads to a slight redshift in the center of the Rayleigh peaks compared with the center of the absorption line, the latter being determined solely by the imaginary part of the optical susceptibility. The shift is typically about 10 meV in magnitude and is largely independent of the chiral angle. We note that a similar importance of the overlap between the real and imaginary parts of the optical susceptibility has also been shown for Raman spectra.[28]

In conclusion, we have calculated the Rayleigh scattering cross section within density-matrix formalism and the tight-binding model. The intensity ratios of the four lowest-lying peaks in the Rayleigh spectra can be explained by the different behavior of the optical matrix element along the two high-symmetry lines $K\Gamma$ and KM. A modeling of the Rayleigh scattering cross section has to consider all allowed subband transitions. The line shape in the Rayleigh spectra exhibits somewhat stronger response at lower energies as a consequence of the nonresonant contributions to the optical susceptibility of higher subband transitions. The latter also leads to a slight redshift in the Rayleigh spectra compared to the absorption spectra. Our results are in good qualitative agreement with experiment. As preliminary calculations show, excitonic effects enhance both the intensity ratios as well as the asymmetry. However, they do not change the described qualitative behavior.

*ermin@itp.physik.tu-berlin.de

[1] S. M. Bachilo, M. S. Strano, C. Kittrell, R. H. Hauge, R. E. Smalley, and R. B. Weisman, Science **298**, 2361 (2002).

[2] Y. Miyauchi, S. Chiashi, Y. Murakami, Y. Hayashida, and S. Maruyama, Chem. Phys. Lett. **387**, 198 (2004).

[3] H. Telg, J. Maultzsch, S. Reich, F. Hennrich, and C. Thomsen, Phys. Rev. Lett. **93**, 177401 (2004).

[4] C. Fantini, A. Jorio, M. Souza, M. S. Strano, M. S. Dresselhaus, and M. A. Pimenta, Phys. Rev. Lett. **93**, 147406 (2004).

[5] M. Y. Sfeir, F. Wang, L. Huang, C.-C. Chuang, J. Hone, S. P. O'Brien, T. F. Heinz, and L. E. Brus, Science **306**, 1540 (2004).

[6] M. Y. Sfeir, T. Beetz, F. Wang, L. Huang, X. M. Henry Huang, M. Huang, J. Hone, S. P. O'Brien, J. A. Misevich, T. F. Heinz, L. Wu, Y. Zhu, and L. E. Brus, Science **312**, 554 (2006).

[7] F. Wang, M. Y. Sfeir, L. Huang, X. M. Henry Huang, Y. Wu, J. Kim, J. Hone, S. O'Brien, L. E. Brus, and T. F. Heinz, Phys. Rev. Lett. **96**, 167401 (2006).

[8] S. Reich, C. Thomsen, and P. Ordejón, Phys. Rev. B **65**, 155411 (2002).

[9] R. Saito, G. Dresselhaus, and M. S. Dresselhaus, Phys. Rev. B **61**, 2981 (2000).

[10] S. Reich and C. Thomsen, Phys. Rev. B **62**, 4273 (2000).

[11] C. F. Bohren and D. R. Huffman, *Absorption and Scattering of Light by Small Particles* (Wiley, New York, 1983).

[12] H. Haug and S. W. Koch, *Quantum Theory of the Optical and Electronic Properties of Semiconductors* (World Scientific, Singapore, 2004).

[13] E. Malić, M. Hirtschulz, F. Milde, A. Knorr, and S. Reich, Phys.

Rev. B **74**, 195431 (2006).

[14] E. Malić, M. Hirtschulz, F. Milde, Y. Wu, J. Maultzsch, T. F. Heinz, A. Knorr, and S. Reich, Phys. Status Solidi B **244**, 4240 (2007).

[15] S. Reich, C. Thomsen, and J. Maultzsch, *Carbon Nanotubes: Basic Concepts and Physical Properties* (Wiley-VCH, Berlin, 2004).

[16] S. Reich, J. Maultzsch, C. Thomsen, and P. Ordejón, Phys. Rev. B **66**, 035412 (2002).

[17] V. N. Popov and L. Henrard, Phys. Rev. B **70**, 115407 (2004).

[18] A. Grüneis, R. Saito, G. G. Samsonidze, T. Kimura, M. A. Pimenta, A. Jorio, A. G. SouzaFilho, G. Dresselhaus, and M. S. Dresselhaus, Phys. Rev. B **67**, 165402 (2003).

[19] J. Jiang, R. Saito, G. G. Samsonidze, A. Jorio, S. G. Chou, G. Dresselhaus, and M. S. Dresselhaus, Phys. Rev. B **75**, 035407 (2007).

[20] R. B. Capaz, C. D. Spataru, S. Ismail-Beigi, and S. G. Louie,

[21] C. D. Spataru, S. Ismail-Beigi, L. X. Benedict, and S. G. Louie, Phys. Rev. Lett. **92**, 077402 (2004).

[22] V. Perebeinos, J. Tersoff, and P. Avouris, Phys. Rev. Lett. **92**, 257402 (2004).

[23] H. Zhao and S. Mazumdar, Phys. Rev. Lett. **93**, 157402 (2004).

[24] M. Hirtschulz, F. Milde, E. Malić, S. Butscher, C. Thomsen, S. Reich, and A. Knorr, Phys. Rev. B **77**, 035403 (2008).

[25] F. Wang, G. Dukovic, L. E. Brus, and T. F. Heinz, Science **308**, 838 (2005).

[26] J. Maultzsch, R. Pomraenke, S. Reich, E. Chang, D. Prezzi, A. Ruini, E. Molinari, M. S. Strano, C. Thomsen, and C. Lienau, Phys. Rev. B **72**, 241402(R) (2005).

[27] S. V. Goupalov, Phys. Rev. B **72**, 195403 (2005).

[28] C. Thomsen and S. Reich, in *Raman Scattering in Carbon Nanotubes in Light Scattering in Solids IX*, edited by M. Cardona and R. Merlin (Springer, New York, 2006).